

Links between nonlinear dynamics and statistical mechanics in a simple one-dimensional model

Hicham Qasmi, Julien Barré and Thierry Dauxois^a

Laboratoire de Physique, UMR-CNRS 5672, ENS Lyon, 46 Allée d'Italie, 69364 Lyon Cédex 07, France

Received: date / Revised version: March 22, 2022

Abstract. We consider the links between nonlinear dynamics and thermodynamics in the framework of a simple nonlinear model for DNA. Two analyses of the phase transition, either with the transfer integral approach or by considering the instability of a nonlinear particular solution, are discussed. Conversely, the computation of the largest Lyapunov exponent is obtained within a thermodynamic treatment. Differences with the Peyrard-Bishop model are also discussed.

Keywords:

Nonlinear dynamics. Statistical physics. Phase Transitions. Lyapunov exponents

PACS.

05.45.-a, 05.70.Fh, 02.40.-k.

1 Introduction

The main goal of the paper is to study the links between the microscopic dynamics and macroscopic thermodynamical properties in a very simplified model for DNA. Both aspects are usually not studied simultaneously; in the literature, the main goal is often, either to consider dynamical aspects of coherent structures (solitons for example) in a system at zero temperature, or to derive thermodynamical properties without really considering the consequences of the existence of these coherent structures. Here, on the contrary, we will put the emphasis on the link and show that both approaches give important insights to the description of the physical properties.

Two aspects will be of particular importance and we would like to shed light on them already in the introduction. A recent method [6], which showed how the stability of a nonlinear solution of the dynamical equations exhibits an interesting approach to describe a phase transition, will be applied in this new model: it will reveal how the small amplitude dynamics needs a careful treatment to adequately describe the thermodynamics. Second, we will describe the relationships between the maximum Lyapunov exponent which characterizes the dynamics and the thermodynamics. Using a geometric method [24], we will explicitly compute the evolution of this dynamical quantity as a function of the temperature: consequences of the phase transition will therefore be explicit. From these calculations, we predict features absent in the Peyrard-Bishop model, although both models are very similar: a

non monotonic behavior of the maximum Lyapunov exponent in the low temperature phase, and a jump at the critical temperature.

In Sec. 2 we present briefly the model. In the following Sec. 3, we show how one can derive its thermodynamical properties. Then, the emphasis is put in Sec. 4 to a special particular solution and on its use to explain the thermodynamical properties. Finally, using the powerful geometric method introduced recently to compute the largest Lyapunov exponent, we discuss in Sec. 5 the link between this dynamical quantity and the phase transition, a thermodynamic concept.

2 The Model

A very simplified model has been proposed in 1989 by M. Peyrard and A. R. Bishop [1] to describe DNA denaturation. This biological phenomenon leads to the breaking of the H-bonds linking both strands of DNA. This process, which appears when either the temperature increases or when the pH of the surrounding solvent is modified, was previously successfully described by Ising models [2]. However, the dynamical properties of the phenomenon were not captured by these static descriptions. This is why, keeping the principle of simplicity, Peyrard and Bishop described this highly complicated biomolecule by two chains of particles coupled by nonlinear springs. This step toward a more complex system, since including the minimal dynamics, was unexpectedly more successful than first understood and have lead to many studies (See Ref. [3] for a review). A large part of the results were interesting from

Send offprint requests to: Thierry Dauxois

^a E-mail:Thierry.Dauxois@ens-lyon.fr

the physical point of view: one may list in particular studies of discrete breathers modes and energy localization in systems involving nonlinear and discreteness effects [4, 5], existence of phase transition in one-dimensional system [6]... Furthermore, several recent results have emphasized that this model could be successfully used to locate promotor regions [7] for real DNA sequences. This unexpected report and similar ones explain why so simple models are still nowadays thought to be possible powerful tools to describe real DNA dynamics.

Two linear chains of particles describing phenomenologically the nucleotides describe the two different strands of DNA as schematically represented in Fig. 1. In the simplest description, all particles of the same chain are harmonically coupled whereas the interstrand interactions are restricted to facing nucleotides; long-range interactions are neglected at this level of description. It is important to understand that because the goal is to describe denaturation dynamics, only transversal degrees of freedom are taken into account. Defined with respect to their equilibrium position, the displacement of the center of mass of the n^{th} nucleotide are called u_n (resp. v_n) for the top (resp. bottom) chain.

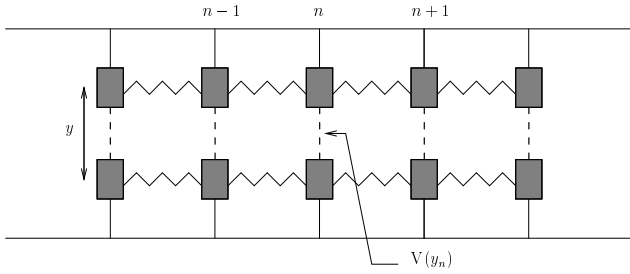


Fig. 1. Schematic presentation of the DNA model.

Denoting p_u the conjugated momentum to the spatial position u and the number of nucleotides being N , the Hamiltonian model can be written as

$$H = \sum_n \left[\frac{p_{u,n}^2}{2m} + \frac{K}{2}(u_n - u_{n-1})^2 + \frac{p_{v,n}^2}{2m} + \frac{K}{2}(v_n - v_{n-1})^2 + V\left(\frac{u_n - v_n}{\sqrt{2}}\right) \right]. \quad (1)$$

The interstrand potential V describes the effective interactions, i.e. in particular hydrogen bonds between base pairs but also the repulsion between phosphates. The canonical transformation $x_n = (u_n + v_n)/\sqrt{2}$ and $y_n = (u_n - v_n)/\sqrt{2}$ decouples simply both degrees of freedom since H can be rewritten as $H = H_x + H_y$ where

$$H_x = \sum_n \left[\frac{p_{x,n}^2}{2m} + \frac{K}{2}(x_n - x_{n-1})^2 \right] \quad (2)$$

and

$$H_y = \sum_n \left[\frac{p_{y,n}^2}{2m} + \frac{K}{2}(y_n - y_{n-1})^2 + V(y_n) \right]. \quad (3)$$

The dynamics and the thermodynamics of the first part, H_x , which corresponds to a linear chain of harmonic oscillators, can be easily computed. We will omit this part in the remaining of the paper without loss of generality. The second part, H_y , on the contrary needs further developments. For the sake of simplicity, we will omit the y index.

The system defined by this hamiltonian H exhibits a second order phase transition as shown in the next section. The low temperature phase corresponds to states where the particles are located close to their equilibrium position, the associated DNA being in the native state: it must correspond to the bottom well of the potential V . On the contrary, in the high temperature phase, DNA being denaturated, the link between facing nucleotides of both strands are broken: consequently, associated particles of the model must be located in a plateau of the potential, far from their equilibrium positions since the force is vanishing. The position in this plateau will be thermodynamically chosen because of the entropy contribution to the free energy, important only at high temperature.

This simple physical description guides therefore the appropriate choice for the potential V . Nevertheless, the analytical calculations that we will present now are possible for only a few cases. The Morse potential $V_m(y) = D(\exp(-a_m y) - 1)^2$ was the first choice [1, 6]. Here, we will present another possible example [8]:

$$V(y) = \begin{cases} -\frac{D}{\cosh^2 ay} & \text{if } y \geq 0 \\ +\infty & \text{if } y < 0. \end{cases} \quad (4)$$

As we will see, the qualitative shapes are really close but the differences of curvatures lead to several consequences. In addition, the impossibility to reach negative values for the variable y gives interesting properties. One important question concerns the influence of the details of the potential V . We will discuss in particular the following points:

- i) values of the critical temperature of the phase transition for both potentials,
- ii) consequences to the related characteristic lengths: order parameter and correlation length,
- iii) largest Lyapunov exponent as a function of temperature.

3 Thermodynamics of the model

3.1 The canonical partition function

As it is well-known nowadays [10, 9], the statistical mechanics of such a one-dimensional short-range Hamiltonian can be exactly derived with the transfer integral method (See appendix A). In the framework of the continuum approximation, the solution relies on solving the following Schrödinger equation

$$-\frac{1}{2\beta^2 K} \frac{d^2 \psi}{dy^2} - \frac{D}{\cosh^2 ay} \psi = \mathcal{E}_k \psi, \quad (5)$$

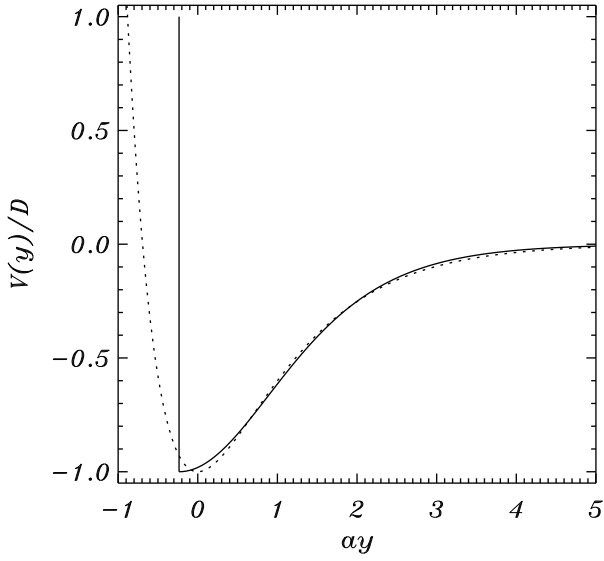


Fig. 2. Comparison between potential (4) (represented by the solid line) with appropriate characteristics (a, y_0) and the Morse potential V/D (dotted line).

if the lattice spacing between sites in the x -direction is set to one.

Defining the quantity

$$\eta = \frac{1}{4} \left[\sqrt{1 + 8 \frac{T_c^2}{T^2}} - 1 \right] \quad (6)$$

where

$$T_c = \frac{\sqrt{KD}}{ak_B}, \quad (7)$$

this equation has $N_\eta = E(\eta + 1/2)$ localized states, with $E(\cdot)$ denoting the integer part. One notes that T_c corresponds to the disappearance of the last discrete state, and will be called the critical temperature.

The $(N_\eta + 1)$ localized states ψ_k can be expressed [8] in terms of hypergeometric functions as

$$\psi_k(y) = \frac{\mathcal{N}_k}{\cosh(ay)^{b_{2k+1}}} F \left(-2k - 1, 2b_{2k+1} + 2k + 2, b_{2k+1} + 1; \frac{e^{-ay}}{e^{-ay} + e^{ay}} \right), \quad (8)$$

where \mathcal{N}_k is the normalization factor of the wave function, $b_n = 2\eta - n$ and finally

$$\mathcal{E}_k = -\frac{a^2}{2\beta^2 K} (2\eta - 2k - 1)^2, \quad (9)$$

the associated eigenvalues.

The ground state which is particularly useful in the remaining of the paper can be simplified as

$$\psi_0(y) = \sqrt{2a \frac{2\eta - 1}{B(2\eta, \frac{1}{2})}} \frac{\sinh ay}{\cosh^{2\eta} ay} \quad (10)$$

by introducing the Euler function

$$B(x, y) = \frac{\Gamma(x+y)}{\Gamma(x)\Gamma(y)} = \int_0^1 dt (1-t)^{x-1} t^{y-1}. \quad (11)$$

3.2 Discussion of the choice of the parameters set

One of the goal of this work is to make a detailed comparison between the Morse potential and potential (4). The parameter set is obtained either by considering the effective physical interactions, or by choosing the values to get the same melting temperature. Assuming that the depth of the potential is known, both possibilities will define a relation between the width of the potentials: a_m^{-1} for the Morse one, and a^{-1} for potential (4).

The choice $a_m \approx 1.472 a$ corresponds to the best fit. On the contrary, as the transition temperature for the Morse potential [1, 11, 9] is $T_c^m = T_c \sqrt{8}$, the second choice $a_m = a\sqrt{8}$ would lead to the same critical temperature. Consequently, when the parameters are fitted, the critical temperature differs by a factor two!

This unexpected disagreement reveals a hidden difference between both potentials: the underlying reason is the important contribution of negative positions y , in the Morse case. They cannot be neglected even if the fast exponential increase was thought to play the role of the impossibility of interpenetration.

The appropriate solution is to introduce an additional parameter. The inverse width a being given by the critical temperature, one could adapt the minimum of the potential to minimize the differences with the Morse potential. A fit restricted to positive y -values over both variables (a_m, y_0) leads to an excellent agreement. This case is presented in Fig. 2 by the solid line.

All results below correspond to the following set of parameters $m = 300$ u. a., $D = 0.00094$ eV, $K = 1.9$ eV.Å⁻² and $a = 4.5$ Å⁻¹. The value of T_c will be different from the Morse case, but both potentials will be very similar as emphasized by Fig. 2. This choice will allow a precise study of the negative y -values region and of the importance of potential curvature for the Lyapunov exponent discussed in section 5.

3.3 Characteristic lengths

As usual, the thermodynamic properties of this system can be characterized by an order parameter, and its fluctuations, in the vicinity of the critical temperature T_c . Here, the appropriate choice is the quantity

$$\ell = \langle \psi_0 | x | \psi_0 \rangle = \int_0^\infty dx x |\psi_0(x)|^2, \quad (12)$$

which diverges for $T = T_c$. This clarifies the name critical temperature which separates, the phase with a finite order parameter (native state) from the phase with infinite order parameter, representing the denaturated state.

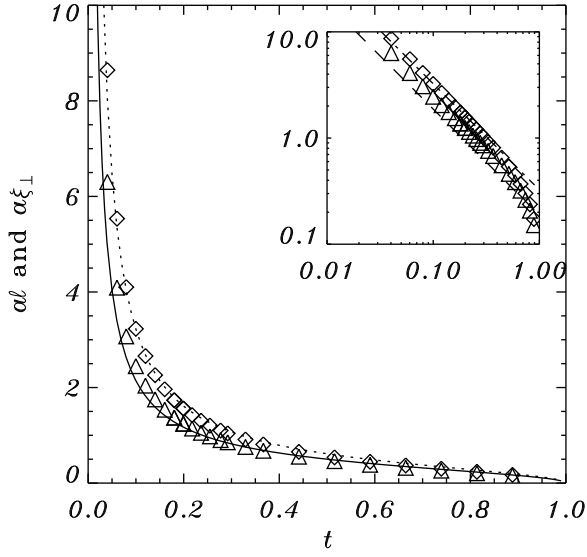


Fig. 3. Order parameter $\alpha\ell$ (solid line and triangles) and correlation length $\alpha\xi_{\perp}$ (dotted line and diamonds) as a function of the reduced temperature $t = 1 - T/T_c$. Lines corresponds to the transfer integral result within the continuum approximation (Eqs. (12) and (14)) whereas symbols correspond to the exact numerical solution of the operator (57). Presented in the inset, the exact numerical data plotted with logarithmic scales emphasize the critical behavior close to the critical temperature. The dashed (resp. dash-dotted) line corresponds to the asymptotic expression (13) (resp. (15)).

The associated critical exponent can even be determined by using the asymptotic expression $\int_0^{\infty} dx x / \cosh^{\alpha} x \stackrel{\alpha \rightarrow 0}{\sim} 1/\alpha^2$. Using expression (10) and introducing the usual reduced temperature $t = 1 - T/T_c$, one finally gets

$$\ell \stackrel{T \rightarrow T_c}{\sim} \frac{3}{16} \frac{1}{a} \frac{1}{|t|}. \quad (13)$$

In agreement with critical phenomena theory, we obtain therefore the usual critical exponent $\beta = -1$, for this second order phase transition. Fig. 3 presents the evolution of ℓ as a function of the temperature. Formula (12), represented with a solid line, agrees very well with the exact result obtained with the discrete transfer operator (57). In the inset, the logarithmic plot emphasizes the critical behavior and confirms the scaling exponent $\beta = -1$.

Interestingly it is also possible to determine the fluctuations of the order parameter which can be computed from the following expression

$$\xi_{\perp}^2 = \langle \psi_0 | (x - \ell)^2 | \psi_0 \rangle. \quad (14)$$

As above, the asymptotic expression can be easily derived by taking into account that $\int_0^{\infty} dx x^2 / \cosh^{\alpha} x \stackrel{\alpha \rightarrow 0}{\sim} 2/\alpha^3$. One thus obtains in the vicinity of the critical temperature that

$$\xi_{\perp} \stackrel{T \rightarrow T_c}{\sim} \frac{3\sqrt{3}}{16} \frac{1}{a} \frac{1}{|t|}. \quad (15)$$

The critical exponent is therefore $\nu_{\perp} = 1$. Fig. 3 shows that the order parameter and its fluctuations are of the

same order in this temperature regime. The inset confirms again the critical behavior and the scaling exponent $\nu = 1$.

It is important to stress that all above analytical results are confirmed by the numerical but exact solution of the transfer integral operator (57), without relying on the continuum approximation: see symbols in Fig 3. As it is nowadays known [6,9], the critical exponents are valid even in the region where discreteness effects can not be neglected. To be more specific, let us introduce the parameter

$$R = \frac{Da^2}{K}, \quad (16)$$

measuring the onsite potential with respect to the elastic coupling. For small value of this parameter, the continuum approximation is valid and results (13) and (15) confirmed. For the set of parameters chosen in this work, R is equal to 10^{-2} , and one get results in values slightly different from Eqs. (13) and (15) for T_c , ℓ , and ξ_{\perp} . However, as shown by Fig. 3 the differences are hardly distinguishable and moreover the critical exponents are fully confirmed.

4 Domain Wall

In the framework of this model, it is also interesting to discuss a new method [6,9], alternative to the usual thermodynamic one proposed in previous section, to detect the phase transition from dynamical considerations. This will illustrate again the importance of the wall located at $y = 0$.

Equations of motion corresponding to Hamiltonian (3) are

$$m\ddot{y}_n = K(y_{n+1} + y_{n-1} - 2y_n) - \frac{\partial V}{\partial y_n} \quad (17)$$

or, in the continuum limit,

$$\ddot{y} = \frac{K}{m} \frac{\partial^2 y}{\partial x^2} - \frac{1}{m} \frac{\partial V}{\partial y}. \quad (18)$$

The uniform profile at the minimum of $V(y)$ is a static solution of the infinite chain with free ends. Profiles verifying $d^2y/dx^2 = 0$ are approximate solutions only on the plateau of the potential, since $\partial V/\partial y$ is close to zero for large y .

There exists also an exact, unbounded, domain-wall like solution

$$y_{DW}^{\pm}(x) = \frac{1}{a} \text{Argsh } e^{\pm z} = \frac{1}{a} \ln \left[e^{\pm z} + \sqrt{1 + e^{\pm 2z}} \right], \quad (19)$$

where $z = \sqrt{2R}(x - x_0)$ and x_0 is an arbitrary constant. Solution (19) represents a configuration which links the stable minimum to a particular member of the metastable configurations, with a slope $\sqrt{2D/K}$. One can easily checks that this corresponds to equal contributions to the elastic and the on-site potential energy densities (D per site). Consequently, the energy of the solution contains a term which is proportional to the number of sites to the right of x_0 and if lattice sites are numbered from 0 to N , one has

$$E_{DW}^{+} = (N - x_0) 2D + \mathcal{O}(N^0) \quad (20)$$

At zero temperature the profile (19) is consequently not stable, and the wall spontaneously move to the right, “zip-ping” back the unbound portion of the double chain. This instability changes however under the influence of temperature.

At non zero temperatures, let us consider small deviations with respect to (19), i.e.

$$y(x, t) = y_{DW}^+(x - x_0) + \sum_j \alpha_j f_j(x - x_0) e^{-i\omega_j t} \quad (21)$$

where $|\alpha_j| \ll a^{-1}$. The linearized eigenfunctions f_j satisfy the Schrödinger-like equation

$$-\frac{d^2 f_j}{dz^2} + \frac{1 - 2e^{2z}}{(1 + e^{2z})^2} f_j = \frac{m\omega_j^2}{2KR} f_j. \quad (22)$$

Eq. (22) has no bound states [8]. There are however scattering states: acoustic phonons oscillating on the flat portion of the potential with frequencies

$$\omega_{ac}^2 = \frac{2K}{m}(1 - \cos q) \quad (23)$$

are some of them.

In the bottom of the well of the potential, let us first forget the wall. Consequently scattering states would be optical phonons with frequencies

$$\omega_{opt}^2 = \frac{2Da^2}{m} + \frac{2K}{m}(1 - \cos q). \quad (24)$$

At finite temperatures, the domain wall would therefore be accompanied by a phonon cloud contributing to the free energy as

$$F_{ph} = k_B T x_0 \int_0^\pi \frac{dq}{\pi} \ln \frac{\omega_{opt}}{\omega_{ac}} + \dots \quad (25)$$

where we omit terms independent of x_0 . Introducing the dispersion relations, we can evaluate [15] the integral in (25) using $\int_0^\pi dx \ln[1 - \cos x + R] = 2\pi \ln[(\sqrt{R} + \sqrt{R+2})/2]$. We obtain thus the total free energy (DW plus phonon cloud)

$$F = \left(k_B T \ln \left[\frac{\sqrt{R} + \sqrt{R+2}}{\sqrt{2}} \right] - 2D \right) x_0 + \text{const.} \quad (26)$$

This result describes in very simple terms why and when the phase transition occurs. At temperatures lower than

$$T_c = \frac{2D}{k_B \ln \left[\sqrt{R/2} + \sqrt{1 + R/2} \right]}, \quad (27)$$

the prefactor of x_0 in Eq. (26) is negative, describing the DW's natural tendency towards high positive values of x_0 : it “zips” the system back to the bound configuration. Conversely, at temperatures higher than T_c , thermal stability is achieved and the DW “opens up”.

It should be noted that the value of T_c predicted by the above DW argument coincides exactly with the result obtained for the Morse potential [6,9]. The limiting behavior in the continuum approximation, i.e. in the limit $R \ll 1$, leads for example to $T_c = 2\sqrt{2KD}/(ak_B)$. This result differs nevertheless from Eq. (7).

Expression (27) is consequently *not* valid for the sech²-potential (4) of interest. The underlying reason is the impossibility of usual phonons to take place in the bottom of the well. The harmonic approximation of the problem leads indeed to a *nonlinear* problem because of the nonlinear condition $y > 0$ introduced by the wall. Optical phonons with frequencies (24) are therefore totally modified by the wall and cannot be computed. A way to take into account this nonlinear condition would consist in selecting only the even modes of optical phonons (24). However, it turns out to be unexact and insufficient. This illustrates again that the presence of the wall strongly modifies the *dynamics* of the system, which leads to important *thermodynamic* consequences.

5 Geometrical method to derive the largest Lyapunov exponent

In the theory of dynamical systems, the concept of *Lyapunov exponent* has also attracted a lot of attention [16, 17] because it defines unambiguously a sufficient condition for chaotic instability. Unfortunately, except for very few systems, it is already an extremely difficult task to derive analytically the expression of the largest one, λ_1 , as a function of the energy density. As some promising results have been recently obtained to describe some properties of high-dimensional dynamical systems [18,19,20, 21,22,23], by combining tools developed in the framework of dynamical systems with concepts and methods of equilibrium statistical mechanics, the idea that both concepts could be related was proposed [24].

5.1 Riemannian geometry approach

The main idea is that the chaotic hypothesis is at the origin of the validity of equilibrium statistical physics, and this fact should be traced somehow in the dynamics and therefore in the largest Lyapunov exponent. The method is based on a reformulation of Hamiltonian dynamics in the language of Riemannian geometry [24]: the trajectories are seen as geodesics of a suitable Riemannian manifold. The chaotic properties of the dynamics are then directly related to the curvature of the manifold and its fluctuations. Indeed, negative curvatures tend to separate initially close geodesics, and thus imply a positive Lyapunov exponent; nevertheless chaos may also be induced by positive curvatures, provided they are fluctuating, through a parametric-like instability. To approximate the curvature felt along a geodesic, the method uses a Gaussian statistical process. The mean value of this process is given by κ_0 and its variance by σ_κ , where κ_0 and σ_κ are the statistical

average of the curvature and its fluctuations, which can be computed by standard methods of statistical mechanics.

Finally one ends up with the following expression of the largest Lyapunov exponent [24]

$$\lambda_1 = \frac{1}{2} \left(\Lambda - \frac{4\kappa_0}{3\Lambda} \right) \quad (28)$$

where

$$\Lambda = \left(\sigma_\kappa^2 \tau + \sqrt{\left(\frac{4\kappa_0}{3} \right)^3 + \sigma_\kappa^4 \tau^2} \right)^{1/3}. \quad (29)$$

In this definition, τ , the relevant time scale associated to the stochastic process, is function of the two following timescales: $\tau_1 \simeq \pi/2\sqrt{\kappa_0 + \sigma_\kappa}$ is the time needed to cover the distance between two successive conjugate points along the geodesics, whereas $\tau_2 \simeq \sqrt{\kappa_0}/\sigma_\kappa$ is related to the local curvature fluctuations. The general rough physical estimate $\tau \simeq (1/\tau_1 + 1/\tau_2)^{-1}$ completes finally the analytical estimate of λ_1 . We continue now by calculating the mean value of the curvature and its fluctuations as a function of the energy density.

5.2 Average curvature

The curvature of the Riemannian manifold is directly given by the Laplacian of the potential. One needs therefore to compute the microcanonical average of the quantity

$$\Delta V = 2KN + 2a^2 D \sum_k g(y_k) \quad (30)$$

and its corresponding fluctuations, where

$$g(y) = \frac{3}{\cosh^4 ay} - \frac{2}{\cosh^2 ay}. \quad (31)$$

We finally obtain

$$\langle \Delta V \rangle_\mu = N (2K + 2a^2 D \langle g(y_k) \rangle_\mu). \quad (32)$$

As, in the thermodynamic limit, ensemble equivalence ensures that averages are equal in all statistical ensembles, we will compute them in the canonical one since the transfer operator method has been shown to be a powerful tool to compute thermodynamic functions, especially if the continuum approximation is valid.

Calculation of Eq. (32) relies on the computation of $\langle g(ay) \rangle_{\text{can}}$, i.e. of terms such as $\langle 1/\cosh^{2\alpha} ay \rangle_{\text{can}}$. Using the transfer operator method in the continuum framework, we immediately find

$$\left\langle \frac{1}{\cosh^{2\alpha} ay} \right\rangle_{\text{can}} = \int_0^\infty dy \frac{1}{\cosh^{2\alpha} ay} |\psi_0(y)|^2. \quad (33)$$

With expression [15]

$$I(\alpha) = \int_0^\infty \frac{dx}{\cosh^{2\alpha} x} = B\left(2\alpha, \frac{1}{2}\right), \quad (34)$$

and the mathematical formula $I(\alpha+1) = I(\alpha)2\alpha/(2\alpha+1)$, canonical averages can be simplified. Introducing the parameter R defined in Eq. (16), one gets

$$\kappa_0 = \frac{\langle \Delta V \rangle_\mu}{N} = 2K \left(1 + 4R \frac{(2\eta-1)(2\eta-3)}{(4\eta+1)(4\eta+3)} \right). \quad (35)$$

Above expression gives in particular the following limiting behaviors

$$\lim_{T \rightarrow 0} \kappa_0 = 2K + 2Da^2 \quad (36)$$

and

$$\lim_{T \rightarrow T_c} \kappa_0 = 2K, \quad (37)$$

which coincide with asymptotic results for the Morse potential [14].

It is however important to notice that expression (35) suggests that the mean curvature is not always positive, its sign being tuned by the value of R . As negative curvatures enhance dynamical instability, this result may have strong consequences on the largest Lyapunov exponent. A careful study [12], shows that for values of R larger than $R_c = (31 + 3\sqrt{105})/8$, expression (35) could be negative in a given interval of temperatures. This result has to be criticized since expression (35) has been derived in the continuum approximation, and one expects important discreteness effects for R values as large as R_c . Numerical, but exact, resolution of the transfer integral operator shows that the curvature is actually positive for all R . Fig. 4 shows the curvature as a function of temperature for the parameter set chosen in this work.

5.3 Fluctuations of the curvature

Contrary to the statistical averages such as the curvature κ_0 , fluctuations are ensembles dependent. This is why one computes first fluctuations in the canonical ensemble, before using the Lebowitz-Percus-Verlet formula [13] to get the microcanonical fluctuations.

In the canonical ensemble, using Eq. (61), fluctuations of expression (30) are given by

$$\frac{\langle \delta^2 \Delta V \rangle}{4a^4 D^2 N} = \frac{1}{N} \sum_{i,j} [\langle g(y_i)g(y_j) \rangle - \langle g(y_i) \rangle \langle g(y_j) \rangle] \quad (38)$$

$$= \sum_l \langle g(y_N)g(y_{N-l}) \rangle - N \langle g(y)^2 \rangle \quad (39)$$

$$= \sum_l \sum_{q=0}^\infty e^{-\beta l(\varepsilon_q - \varepsilon_0)} \left| \int dy g(y) \psi_q^*(y) \psi_0(y) \right|^2 - N \langle g(y)^2 \rangle \quad (40)$$

$$= \sum_l \sum_{q=1}^\infty e^{-\beta l(\varepsilon_q - \varepsilon_0)} \left| \int dy g(y) \psi_q^*(y) \psi_0(y) \right|^2 \quad (41)$$

$$\stackrel{N \rightarrow \infty}{\sim} \sum_{q=1}^\infty \frac{1}{1 - e^{-\beta(\varepsilon_q - \varepsilon_0)}} \left| \int dy g(y) \psi_q^*(y) \psi_0(y) \right|^2 \quad (42)$$

Above expression can be used to compute the canonical fluctuations.

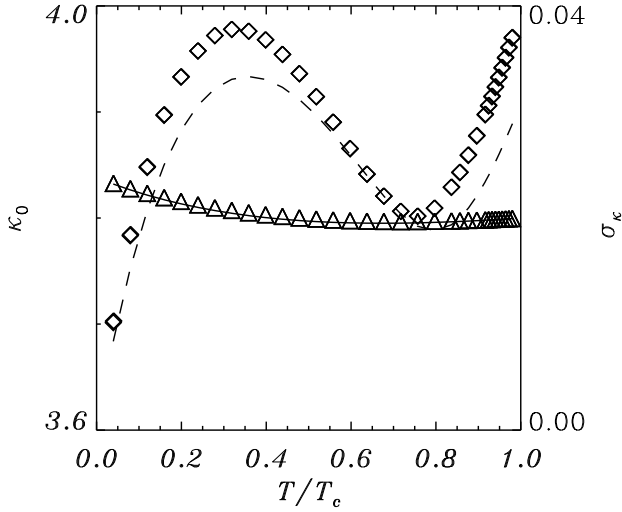


Fig. 4. Average curvature κ_0 and canonical fluctuations σ_κ versus temperature. The triangles (resp. diamonds) represent the exact numerical result for the curvature (resp. canonical fluctuations), obtained with the transfer integral formalism. The solid line corresponds to analytical formula (35) whereas the dashed line correspond to the microcanonical fluctuations (47).

The microcanonical fluctuations will finally be recovered by using the Lebovitz-Percus-Verlet formula [13]. For any quantity C with fluctuations $\langle \delta^2 C \rangle$, both fluctuations are related through the formula

$$\langle \delta^2 C \rangle_\mu = \langle \delta^2 C \rangle_{\text{can}} + \frac{\partial \langle U \rangle_{\text{can}}}{\partial \beta}^{-1} \left(\frac{\partial \langle C \rangle_{\text{can}}}{\partial \beta} \right)^2, \quad (43)$$

where $\langle U \rangle_{\text{can}}$ is the averaged energy of the system.

The canonical partition function Z being the product of a kinetic part Z_T and a configurational one Z_c , the averaged energy is given by

$$\langle U \rangle_{\text{can}} = -\frac{\partial \ln Z_T}{\partial \beta} - \frac{\partial \ln Z_c}{\partial \beta}. \quad (44)$$

The first contribution is as usual $N/(2\beta)$ whereas the last one, can be simplified in the continuum approximation by using the transfer integral method (See Appendix A and in particular Eq. (60)). Denoting ε_0 the ground state of the associated Schrödinger equation, one obtains $\ln Z_c = -N\beta\varepsilon_0$ with

$$\varepsilon_0 = \frac{1}{2\beta} \ln \frac{\beta K}{2\pi} - \frac{a^2}{2K\beta^2} (2\eta - 1)^2. \quad (45)$$

The averaged energy is therefore

$$\langle U \rangle_{\text{can}} = N \left[\frac{1}{2\beta} + \frac{\partial(\beta\varepsilon_0)}{\partial \beta} \right]. \quad (46)$$

The final analytical expression for the microcanonical fluctuations is not simple. Introducing quantities $\beta_c = 1/(k_B T_c)$ and $\delta = T_c/T$, one gets

$$\begin{aligned} \frac{\langle \delta^2 \kappa_0 \rangle_\mu - \langle \delta^2 \kappa_0 \rangle_{\text{can}}}{18432a^4 D^2 K \beta_c} = & -\delta^5 \left(-16\delta^2 + 7\sqrt{1+8\delta^2} + 5 \right)^2 \\ & / (1+8\delta^2)^{\frac{3}{2}} / \left(2 + \sqrt{1+8\delta^2} \right)^4 \\ & / (16K\beta_c \delta^3 \sqrt{1+8\delta^2} - 36a^2 \delta^2 \\ & + 40a^2 \delta^2 \sqrt{1+8\delta^2} + 2K\beta_c \delta \\ & \sqrt{1+8\delta^2} - 3a^2 + 5a^2 \sqrt{1+8\delta^2}). \end{aligned} \quad (47)$$

Above expressions (42) and (47) can be combined to compute the microcanonical fluctuations. This is what has been performed to plot the fluctuations of the curvature in Fig. 4.

Close to the critical temperature T_c , the continuum part of the transfer operator spectrum should be taken into account and an explicit analytical calculation is possible in principle but particularly tedious. On the contrary, one can simplify above expression in the low temperature regime as shown in next section.

5.4 Low temperature estimate

In the low temperature regime by replacing the prefactor $(1 - \exp[-\beta(\varepsilon_q - \varepsilon_0)])^{-1}$ by 1 in Eq. (42), one finally gets

$$\langle \delta^2 \Delta V \rangle_{\text{can}} \simeq 4Na^4 D^2 \sum_{q=1}^{\infty} \langle \psi_q | g | \psi_0 \rangle \langle \psi_0 | g | \psi_q \rangle \quad (48)$$

$$= 4Na^4 D^2 \left[\langle \psi_0 | g^2 | \psi_0 \rangle - \langle \psi_0 | g | \psi_0 \rangle^2 \right]. \quad (49)$$

Combining result

$$\langle \psi_0 | g^2 | \psi_0 \rangle = 16 \frac{2\eta(2\eta-1)(4\eta^2-6\eta+11)}{(4\eta+1)(4\eta+3)(4\eta+5)(4\eta+7)} \quad (50)$$

with formula (35), one ends up with

$$\langle \delta^2 g \rangle_{\text{can}} = 48 \frac{(2\eta-1)(256\eta^3-184\eta+105)}{(4\eta+1)^2(4\eta+3)^2(4\eta+5)(4\eta+7)}. \quad (51)$$

As the microcanonical correction (47) can be neglected in this region, the microcanonical fluctuations of the curvature are finally given in the low temperature regime by

$$\sigma_\kappa^2 = \frac{\langle \delta^2 \Delta V \rangle_{\text{can}}}{N} \quad (52)$$

$$\simeq 4D^2 a^4 \frac{48(2\eta-1)(256\eta^3-184\eta+105)}{(4\eta+1)^2(4\eta+3)^2(4\eta+5)(4\eta+7)}. \quad (53)$$

This expression can be used in the low temperature region to get a simpler expression for the largest Lyapunov exponent. One thus obtain that it increases quadratically with the temperature.

5.5 Largest Lyapunov exponent

We can now estimate the largest Lyapunov exponent λ_1 for this high-dimensional system of N coupled particles in the external sech^2 -potential (4).

As κ_0 is positive, the instability of trajectories is due to fluctuations of curvatures as reported by Pettini, Casetti and Cohen [24]. Analytical expressions (35) for κ_0 and (53) for σ_κ were the only missing points in the estimate (28) for λ_1 . One can in addition notes that in the low temperature region, where $\sigma_\kappa \ll \kappa_0$ as attested by Fig. 4, one gets the asymptotic expression

$$\lambda_1 \simeq \frac{\pi}{8} \frac{\sigma_\kappa^2}{\kappa_0^{\frac{3}{2}}}. \quad (54)$$

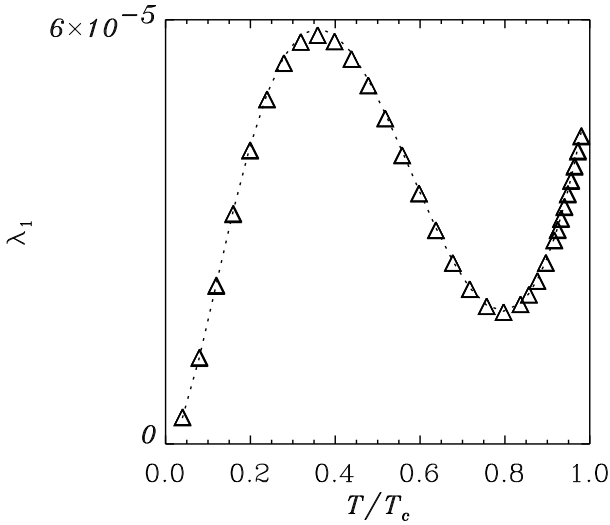


Fig. 5. Largest Lyapunov exponent λ_1 versus T/T_c . The triangles correspond to the transfer integral result, whereas the dotted line correspond to the analytical expression (54).

Fig. (5) presents the temperature evolution of the largest Lyapunov exponents. Two features should be emphasized in comparison to what has been previously reported for the Morse potential [14]. One can notice a local maximum and a local minimum of the Lyapunov exponent in the low temperature region. More importantly, one has to realize that for temperatures larger than the critical one T_c , particles are on the plateau of the potential; the chain being equivalent to a linear chain, the largest Lyapunov exponent λ_1 if of course zero. The Lyapunov exponent should thus present a jump close to the critical temperature. It is important to check these two strong predictions by considering careful microcanonical numerical simulations with large systems. This would provide a precise test of the geometrical method to calculate Lyapunov exponents.

6 Conclusion

We have presented a new qualitative model for DNA denaturation directly inspired by previous works [1, 11, 6]. Its complete statistical mechanics was derived, as well as all features related to the second order phase transition: not only the critical temperature, but also the critical exponents related to the order parameter and the transversal correlation length.

We have in particular emphasized the important role of the negative y -values for the Morse potential which were believed to be unimportant [11]. If critical exponents are of course not affected, the critical temperature is strongly dependent on it. Furthermore, using a geometric approach to estimate the largest Lyapunov exponent, we have computed its evolution as a function of the temperature. The results are unexpectedly qualitatively different from those obtained with the Morse potential.

This work has been partially supported by the French Ministère de la Recherche grant ACI jeune chercheur-2001 N° 21-31, and the Région Rhône-Alpes for the fellowship N° 01-009261-01.

A Transfer integral method for the canonical partition function

With periodic boundary conditions, $y_0 = y_N$, the configurational partition function of Hamiltonian (3) can be written as

$$Z_c = \int \prod_{i=0}^N dy_i e^{-\beta f(y_i, y_{i-1})} \delta(y_0 - y_N) \quad (55)$$

by introducing the symmetric function

$$f(y_n, y_{n-1}) = -\frac{D}{2} \left[\frac{1}{\cosh^2 ay_n} + \frac{1}{\cosh^2 ay_{n-1}} \right] + \frac{K}{2} (y_n - y_{n-1})^2. \quad (56)$$

Defining the transfer operator T as

$$T[\phi](y) = \int_{\mathbb{R}} dx \phi(x) e^{-\beta f(y, x)}, \quad (57)$$

its eigenvalues ε_k and normalized eigenvectors ψ_k are given by $T[\psi_k] = \exp(-\beta \varepsilon_k) \psi_k$.

Introducing the orthonormalization condition

$$\delta(y - y_0) = \sum_k \psi_k^*(y_0) \psi_k(y) \quad (58)$$

in Eq. (55), one gets [9]

$$Z_c = \sum_k e^{-N \beta \varepsilon_k}. \quad (59)$$

If the lowest eigenvalue ε_0 is discrete and located in the gap below the continuum, one can simplify above expression in the limit $N \rightarrow \infty$, so that

$$Z_c \simeq e^{-N \beta \varepsilon_0}. \quad (60)$$

A similar method to compute the canonical average of any function $h(y)$ leads to the following result

$$\langle h(y) \rangle_{\text{can}} = \langle h(y_N) \rangle_{\text{can}} \underset{N \rightarrow \infty}{\simeq} \int dy h(y) |\psi_0(y)|^2. \quad (61)$$

Above results are valid without approximations. However, applying the continuum approximation, it is possible to go one step further since there is a mapping [11, 9] between the transfer integral operator and the following Schrödinger equation

$$-\frac{1}{2\beta^2 K} \frac{d^2 \psi}{dy^2} - \frac{D}{\cosh^2 ay} \psi = \mathcal{E}_k \psi. \quad (62)$$

As the spectrum of a quantum particle in the potential (4) is known, one can derive the analytical expression of (61) within this approximation.

References

1. M. Peyrard, A. R. Bishop, *Physical Review Letters* **62**, 2755-2758 (1989).
2. R. M. Wartell, A. S. Benight, *Physics Reports* **126**, 67-107 (1985).
3. M. Peyrard, *Nonlinearity* **17**, R1-R40 (2004).
4. T. Dauxois, M. Peyrard, A. R. Bishop, *Physical Review E* **47**, 684-695 (1993).
5. T. Dauxois, M. Peyrard, *Physical Review Letters* **70**, 3935-3938 (1993).
6. T. Dauxois, N. Theodorakopoulos, M. Peyrard, *Journal of Statistical Physics* **107**, 869-891 (2002).
7. C. H. Choi, G. Kalosakas, K. O. Rasmussen, M. Hiromura, A. R. Bishop, A. Usheva, *Nucleic Acids Research* **32**, 1584-1590 (2004).
8. P.M. Morse, H. Feshbach, *Methods of Theoretical Physics*, Mc Graw-Hill Book Company (1953).
9. M. Peyrard, T. Dauxois, *Physique des Solitons*, CNRS Éditions-EDP Sciences (2004).
10. J. A. Krumhansl, J. R. Schrieffer, *Physical Review B* **11**, 3535-3545 (1975).
11. T. Dauxois, *Dynamique non-linéaire et mécanique statistique d'un modèle d'ADN*, PhD thesis, Université de Bourgogne (1993).
12. H. Qasmi, Rapport de maîtrise, "Lien entre dynamique et thermodynamique autour d'un modèle simple d'ADN", ENS Lyon (2003).
13. J.L. Lebowitz, J.K. Percus, L. Verlet, *Physical Review* **153**, 250-254 (1967).
14. J. Barré, T. Dauxois, *Europhysics Letters* **55**, 164-170 (2001).
15. I.S. Gradshteyn, I.M. Ryzhik, *Table of Integrals, Series, and Products, Fifth Edition*, Academic Press (1994).
16. P. Manneville, *Structures Dissipatives, Chaos et Turbulence*, Aléa Saclay (1991).
17. A. J. Lichtenberg, M. A. Lieberman, *Regular and Chaotic Dynamics*, Springer, Berlin (1992).
18. L. Casetti, R. Livi, M. Pettini, *Physical Review Letters* **74**, 375-378 (1995).
19. V. Constantoudis, N. Theodorakopoulos, *Physical Review E* **55**, 7612-7618 (1997).
20. V. Latora, A. Rapisarda, S. Ruffo *Physica D* **131**, 38-54 (1999).
21. M. C. Firpo, *Physical Review E* **57**, 6599-6603 (1998).
22. R. O. Vallejos, C. Anteneodo *Physical Review E* **66**, 021110 (2002). C. Anteneodo, R. N. P. Maia, R. O. Vallejos, *Physical Review E* **68**, 036120 (2003). R. O. Vallejos, C. Anteneodo *Physical Review E* **66**, 021110 (2002).
23. S. Tanase-Nicola, J. Kurchan, *J. Phys. A-Math Gen.* **36**, 10299-10324 (2003).
24. L. Casetti, M. Pettini, E.G.D Cohen, *Physics Reports* **337**, 237-341 (2000).